Exo70 Isoform Switching upon Epithelial-Mesenchymal Transition Mediates Cancer Cell Invasion

Hezhe Lu,[1] Jianglan Liu,[1] Shujing Liu,[2] Jingwen Zeng,[1] Deqiang Ding,[5] Russ P. Carstens,[3,4] Yusheng Cong,[5] Xiaowei Xu,[2] and Wei Guo[1,*]

[1]Department of Biology, School of Arts and Sciences
[2]Department of Pathology and Laboratory Medicine, Perelman School of Medicine
[3]Department of Medicine, Perelman School of Medicine
[4]Department of Genetics, Perelman School of Medicine
University of Pennsylvania, Philadelphia, PA 19104, USA
[5]Institute of Aging Research, Hangzhou Normal University School of Medicine, Hangzhou 311121, China
*Correspondence: guowei@sas.upenn.edu
http://dx.doi.org/10.1016/j.devcel.2013.10.020

SUMMARY

Epithelial-mesenchymal transition (EMT) is an important developmental process hijacked by cancer cells for their dissemination. Here, we show that Exo70, a component of the exocyst complex, undergoes isoform switching mediated by ESRP1, a pre-mRNA splicing factor that regulates EMT. Expression of the epithelial isoform of Exo70 affects the levels of key EMT transcriptional regulators such as Snail and ZEB2 and is sufficient to drive the transition to epithelial phenotypes. Differential Exo70 isoform expression in human tumors correlates with cancer progression, and increased expression of the epithelial isoform of Exo70 inhibits tumor metastasis in mice. At the molecular level, the mesenchymal—but not the epithelial—isoform of Exo70 interacts with the Arp2/3 complex and stimulates actin polymerization for tumor invasion. Our findings provide a mechanism by which the exocyst function and actin dynamics are modulated for EMT and tumor invasion.

INTRODUCTION

Epithelial-mesenchymal transition (EMT) is an important developmental process by which epithelial cells of apical-basolateral polarity convert to migratory mesenchymal state (Yang and Weinberg, 2008; Thiery et al., 2009). EMT is essential for embryogenesis and organ formation and is often hijacked by tumor cells to achieve their efficient dissemination to distant organs (Nieto, 2011; Thiery et al., 2009; Valastyan and Weinberg, 2011; Yang and Weinberg, 2008). Years of intensive research in the field have demonstrated that transcriptional regulations involving such factors as Snail, Twist, and ZEB1/2 are required for cancer EMT (Huber et al., 2005; Thiery, 2002; Yang and Weinberg, 2008). Recently, accumulating evidence indicates that alternative splicing also plays a significant role in EMT, with epithelial and mesenchymal cells carrying distinct alternative splicing signatures. ESRP1 and ESRP2 are key splicing factors that regulate the mesenchymal-to-epithelial transition (MET) and govern the critical isoform switching events of a spectrum of genes that are involved in intracellular signaling, cell-cell adhesion, and cytoskeleton rearrangement (Dittmar et al., 2012; Shapiro et al., 2011; Warzecha and Carstens, 2012; Warzecha et al., 2009, 2010). However, how alternative splicing affects the functions of protein isoforms to impact EMT or MET is poorly understood.

The exocyst is an octameric protein complex consisting of Sec3, Sec5, Sec6, Sec8, Sec10, Sec15, Exo70, and Exo84 that are evolutionarily conserved from yeast to human. The exocyst is essential for polarized exocytosis and plasma membrane expansion (He and Guo, 2009; Hsu et al., 2004; Munson and Novick, 2006). Recent studies have demonstrated that the exocyst is involved in cell migration (Liu et al., 2009; Ren and Guo, 2012; Rossé et al., 2006; Spiczka and Yeaman, 2008; Thapa et al., 2012; Zuo et al., 2006; Zhao et al., 2013). In particular, the exocyst subunit Exo70 directly interacts with the Arp2/3 complex during cell migration (Liu and Guo, 2012; Liu et al., 2009; Zuo et al., 2006). Besides cell migration, the exocyst is also implicated in the establishment of epithelial apical-basolateral asymmetry. Components of the exocyst were shown to be recruited to adherens junctions, and disruption of the exocyst function affected the formation of epithelia (Bryant et al., 2010; Grindstaff et al., 1998; Yeaman et al., 2004). The establishment of epithelial asymmetry and directional cell migration are thought to be contrasting states that directly impact EMT. How the exocyst paradoxically promotes these two seemingly opposite cellular processes is intriguing.

In this study, we identify and characterize Exo70 as an important splicing target of ESRP1. Interestingly, selective expression of a single Exo70 isoform affects the expression of transcription factors such as Snail and ZEB2 and leads to cellular transitions between epithelial and mesenchymal phenotypes. In humans, differential expression of Exo70 isoforms correlates with breast tumor progression. At the molecular level, Exo70 isoforms exhibit distinct abilities to interact with
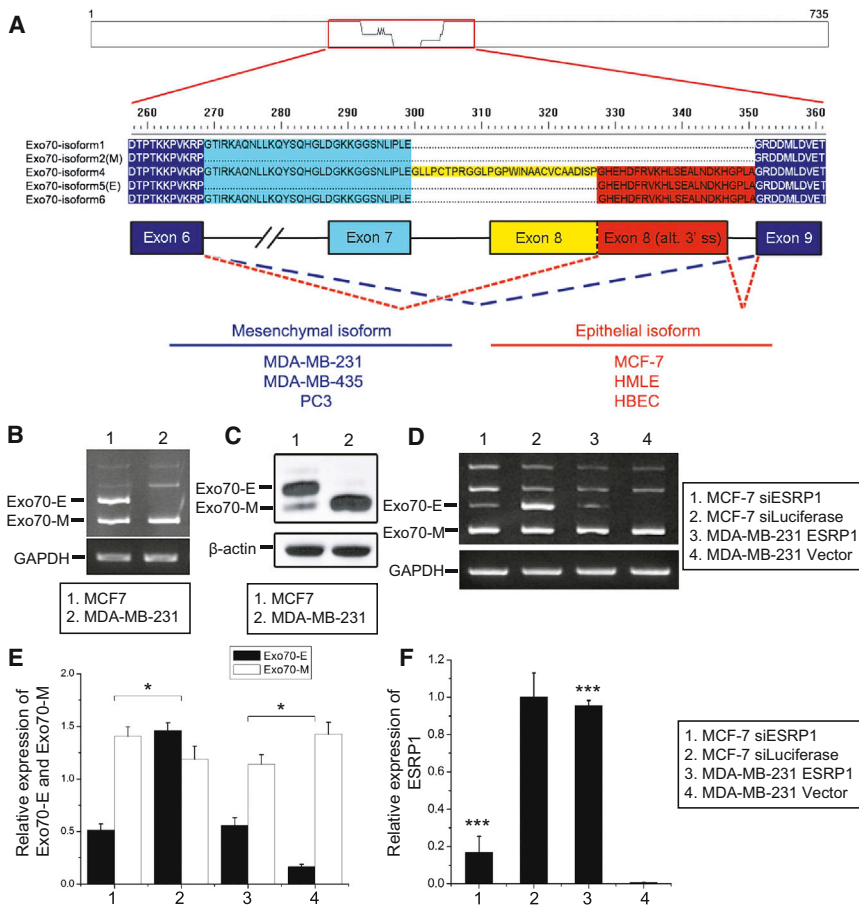
Figure 1. ESRP1 Mediates the Alternative Splicing of Exo70

(A) The mesenchymal (Exo70-M) and epithelial (Exo70-E) isoforms of Exo70 are indicated. Different exons in the variable region of Exo70 are shown by different colors. Comparing Exo70-M and Exo70-E, Exo70-E contains a 23-amino-acid insertion that is part of Exon 8 generated by ESRP-mediated alternative splicing.

(B and C) The expression of Exo70 isoforms in MCF-7 (epithelial) and MDA-MB-231 cells (mesenchymal) was examined by RT-PCR (B) and western blot using an anti-Exo70 antibody that recognizes both isoforms in the cell (C).

(D) RT-PCR analysis of Exo70 isoforms in MCF-7 cells treated with ESRP1 siRNA (left) or in MDA-MB-231 cells overexpressing ESRP1 (right).

(E) Quantification of Exo70-M and Exo70-E mRNA levels in cells used in (D). The expression levels of Exo70 isoforms were normalized to GAPDH. n = 3. *p < 0.05.

(F) ESRP1 expression levels in cells used in (D) were examined by qPCR. Relative expression levels of ESRP1 were normalized to MCF-7 control cells. n = 3. ***p < 0.001.

Student's t test was performed using software R, version 2.14. Error bars indicate SD. See also Figure S1.

claudin-low, invasive breast cancer cell line MDA-MB-231. This observation was further confirmed by western blot analysis with an anti-Exo70 monoclonal antibody that recognizes both isoforms of Exo70 (Figure 1C).

Epithelial splicing regulatory proteins 1 and 2 (ESRP1 and ESRP2) have recently been identified as important regulators of EMT due to their role in orchestrating splicing events in a wide range of proteins involved in cell adhesion and migration (Warzecha et al., 2009, 2010). Exo70 was identified as one of the top candidates that are spliced by ESRP1 and ESRP2 (Warzecha et al., 2010). Here, we examined the regulation of Exo70 isoform expression by ESRP1 in epithelial and mesenchymal cells (Figures 1D–1F). In MCF-7 cells, when ESRP1 expression was silenced by siRNA, the level of Exo70-E was significantly decreased. Conversely, in MDA-MB-231 cells, where the expression of endogenous ESRP1 level is low, ectopic expression of ESRP1 led to an increase in Exo70-E expression.

the Arp2/3 complex and stimulate actin polymerization for cell invasion. Our study not only reveals a role of Exo70 in EMT but also demonstrates that specific expression of a splicing isoform can be both a consequence and regulatory factor during this critical transition. Our results suggest the interplays among different regulatory paradigms (transcription and RNA splicing) of EMT. Finally, our study indicates that alternative splicing can be used to effectively switch the function of an evolutionarily conserved protein for very different cellular processes such as epithelial formation and mesenchymal migration.

RESULTS

ESRP1 Mediates the Alternative Splicing of Exo70

Human cells have five Exo70 isoforms that differ in a region located in the middle of the proteins. Using PCR primers flanking the variable region, we examined the relative expression of these 5 Exo70 isoforms in a number of human cell lines (Figure S1 available online). As the expression patterns of Exo70 isoforms 2 and 5 (henceforth referred to as "Exo70-M" and "Exo70-E," respectively) (Figure 1A) consistently display a correlation with the mesenchymal or epithelial phenotype, they thereafter became the focus of our study. As shown in Figure 1B, Exo70-E mRNA is highly expressed in the luminal epithelial breast carcinoma cell line MCF-7 but not in the

Exo70 Isoform Switching during EMT

To examine the expression of Exo70 isoforms during EMT, we used Twist1-ER-transfected human mammary epithelial (HMLE) cells, a well-established inducible EMT model (Eckert et al., 2011; Mani et al., 2008; Yang et al., 2004). Notably, during 14 days of EMT induction by tamoxifen (TAM), the level of Exo70-E gradually diminished, whereas the level of Exo70-M slightly increased as detected by RT-PCR (Figures 2A and 2B). As positive controls, the downregulation of the epithelial marker E-cadherin and upregulation of the mesenchymal marker N-cadherin were observed along the time course of TAM treatment (Figure 2A). Using quantitative PCR (qPCR), we found that the
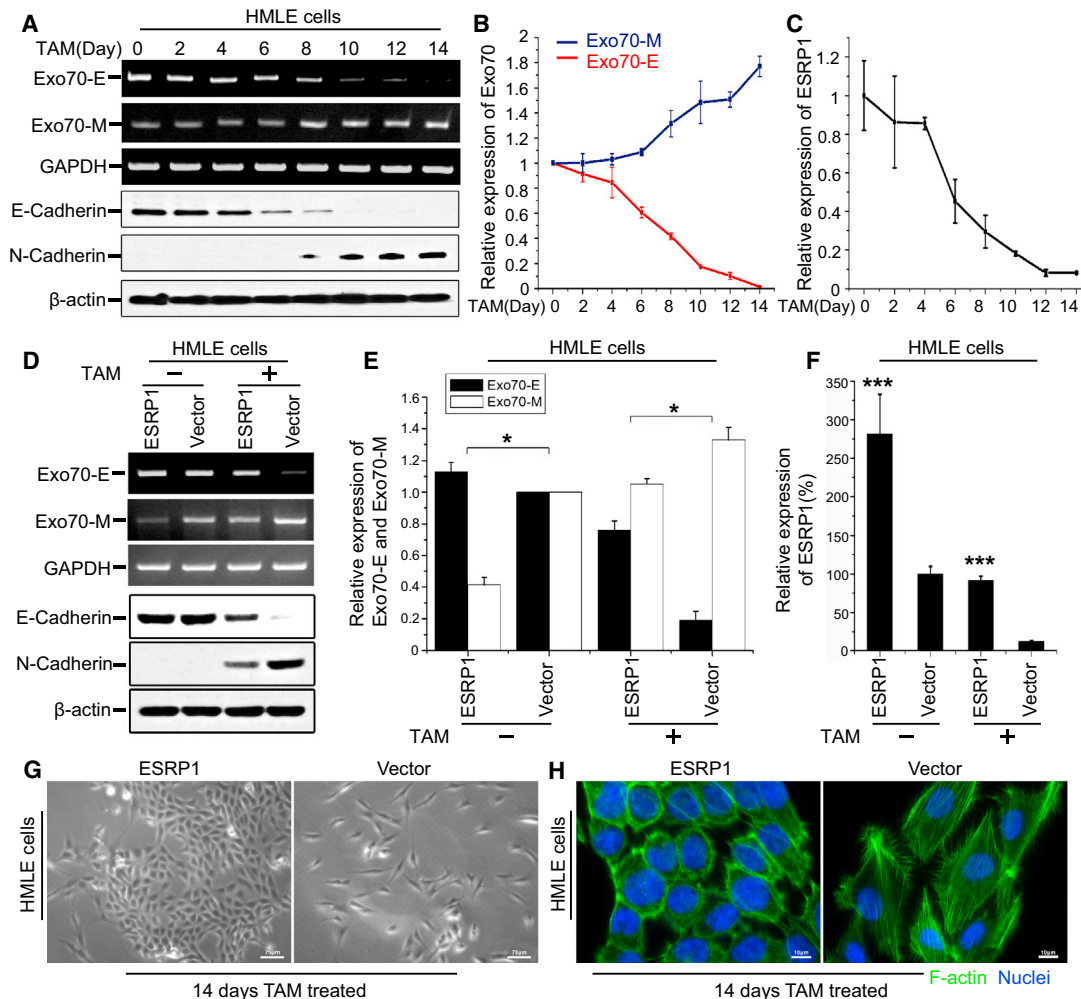
Figure 2. Exo70 Isoform Switching during EMT

(A) RT-PCR analysis of mRNA levels of Exo70-E and Exo70-M during TAM-induced EMT in HMLE/Twist-ER cells. Specific primers that only amplified Exo70-E or Exo70-M sequences were used. GAPDH was used as an internal control. The expression levels of E-cadherin and N-cadherin were examined by western blot, which confirmed that the HMLE/Twist-ER cells had undergone EMT. β-actin was used as a protein loading control.

(B) Quantification of Exo70-M and Exo70-E mRNA levels in HMLE/Twist-ER cells used in (A). The expression levels of Exo70 isoforms in TAM-treated cells were normalized to untreated cells.

(C) ESRP1 expression levels in HMLE/Twist-ER cells used in (A) were examined by qPCR. ESRP1 expression levels in TAM-treated cells were normalized to untreated cells.

(D) RT-PCR analysis of Exo70-E and Exo70-M levels in HMLE/Twist-ER cells (TAM treated or untreated) overexpressing ESRP1. The expression levels of E-cadherin and N-cadherin in these cells were examined by western blot. Cells transfected with vector alone were used as a negative control.

(E) Quantification of Exo70-M and Exo70-E mRNA levels in cells used in (D). The expression levels of Exo70 isoforms were normalized to TAM-untreated control cell. *p < 0.05.

(F) ESRP1 expression levels in cells used in (D) were examined by qPCR. Relative expression levels of ESRP1 were normalized to untreated HMLE-control cells. ***p < 0.001.

(G) Phase-contrast images of ESRP1-induced morphological changes in HMLE-Twist cells after 14 days of TAM treatment. Scale bar, 75 μm.

(H) Alexa-488-phalloidin staining (green) showing ESRP1-induced actin cytoskeleton change in HMLE-Twist cells after 14 days of TAM treatment. Nuclei were stained with DAPI (blue). Scale bar, 10 μm.

Student's t test was performed using software R, version 2.14. Error bars indicate SD.

expression of ESRP1 decreased correspondingly with Exo70-E expression (Figure 2C). To test whether ESRP1 is involved in the regulation of Exo70 isoform switching during EMT, we infected HMLE/Twist1-ER cells with ESRP1, then treated these cells with TAM. While the Exo70-E level in TAM-treated cells infected with vector (as a control) had a much reduced level of Exo70-E, cells infected with ESRP1 exhibited a high level of Exo70-E expression (Figures 2D–2F). Furthermore, ESRP1 expression prevented TAM-induced HMLE/Twist-ER cells from undergoing EMT, as indicated by the retention of the epithelial marker E-cadherin, as well as blunted upregulation of the mesenchymal marker N-cadherin compared with vector control

(Figure 2D). Microscopy analyses showed that expression of ESRP1 changed the cell morphology and actin organization that happens during normal EMT (Figures 2G and 2H). Taken together, these results suggest that ESRP-mediated Exo70 isoform switching takes place during EMT.

Expression of Exo70-E in MDA-MB-231 Cells Induces an Epithelial Cell-like Phenotype

We next determined whether increased expression of Exo70-E or Exo70-M could affect cell morphology. To this end, we generated MDA-MB-231 cell lines stably expressing green fluorescent protein (GFP)-tagged Exo70-E or Exo70-M. As shown in Figure 3A, MDA-MB-231 cells expressing GFP-Exo70-M or GFP vector alone retained dispersed and mesenchymal properties, with migratory leading edges indicated by actin staining. In contrast, MDA-MB-231 cells expressing GFP-Exo70-E changed from their original mesenchymal morphology to a cobblestone-like epithelial morphology characterized by cell-cell adhesion and compact cell clusters (Figure 3A; see also Figure 6E). As MDA-MB-231 cells do not have detectable levels of E-/N-cadherin, but instead express cadherin-11 and β-catenin (Feltes et al., 2002; Nieman et al., 1999), we examined β-catenin localization by immunofluorescence microscopy. As shown in Figure 3B and quantified in Figure S2A, β-catenin was distributed in the cytoplasm and nucleus in MDA-MB-231 cells expressing GFP-Exo70-M or GFP. In cells expressing GFP-Exo70-E, however, β-catenin was recruited to sites of cell-cell contact along the entire cell periphery, suggesting that Exo70-E is capable of inducing mesenchymal cells to acquire epithelial-like properties.

Next, we examined the migration properties of MDA-MB-231 cells by wound healing assays (Figures 3C and 3D). We have previously generated siRNA oligos that selectively knock down Exo70 (Zuo et al., 2006; Liu et al., 2007, 2009). Here, we found that cells with their endogenous Exo70 knocked down by siRNA took more time for wound closure than control cells. These cells, when expressing siRNA-resistant Exo70-M, regained their migration velocity. In contrast, expression of Exo70-E inhibited the migration of MDA-MB-231 cells. We have also performed the transwell assay to examine the motility of these cells. As shown in Figure 3E, while expression of Exo70-E in Exo70 knockdown MDA-MB-231 cells failed to rescue the motility defect, expression of Exo70-M promoted cell motility. Our data suggest that the Exo70-M isoform is involved in MDA-MD-231 cell migration, and the inhibitory phenotype of Exo70-E probably results from its effect on epithelial cell-like transition.

To investigate the impact of Exo70-M on epithelial cells, we expressed GFP-Exo70-M in HMLE cells. As shown in Figures 3H and 3I, HMLE cells ectopically expressing Exo70-M tended to lose the cell-cell junctions and appeared to be more expanded and dispersed. E-cadherin and β-catenin became less associated with the plasma membrane at the regions of cell-cell contact. On the other hand, expression of GFP-Exo70-E or GFP alone had no effect.

The observation that expression of a single Exo70 isoform led to the transition between the epithelial and mesenchymal phenotypes is striking. We therefore determined whether the expression of Exo70-E and Exo70-M affects the mRNA levels of the key EMT-inducing transcription factors, including Snail and ZEB2 (Huber et al., 2005; Thiery, 2003). As shown in Figures 3F and 3G, while Exo70-M expression did not have marked effects on the levels of Snail and ZEB2 in MDA-MD-231 cells, Exo70-E expression led to a significant reduction of the mRNA levels of both transcription factors. Furthermore, expression of Exo70-E induced a significant upregulation of Snail and ZEB2 target genes (Figure S2B). This result suggests that Exo70-E, though a splicing product of ESRP1, can in turn function as a potential EMT and/or MET inducer.

Exo70-M, but Not Exo70-E, Promotes Tumor Cell Invasion In Vitro

The EMT initiates tumor cell invasion, which leads to cancer metastasis. We thus investigated the role of Exo70-E and Exo70-M in tumor cell invasion. First, the invasiveness of MDA-MB-231 cells was examined by transwell assays using matrigel-coated Boyden chambers. Cells with their endogenous Exo70 knocked down by siRNA were much less invasive (Figure 4A). When transfected with siRNA-resistant Exo70-M, these cells regained their invasiveness. In contrast, expression of Exo70-E failed to rescue the invasive property.

Invadopodia are cell membrane protrusions that extend to the extracellular matrix (ECM). Invadopodia promote tumor cell invasion and cancer metastasis by actin polymerization and degradation of the ECM (Gimona et al., 2008; Linder, 2007; Murphy and Courtneidge, 2011; Nürnberg et al., 2011; Weaver, 2006; Yamaguchi et al., 2005). We have investigated the role of Exo70-E and Exo70-M in invadopodia activity by expressing different Exo70 isoforms in c-Src Y527F-transfected MDA-MB-231 cells ("MDA-MB-231-Src") with siRNA knockdown of the endogenous Exo70. The invadopodia activities of these cells were examined by their ability to digest fluorescence-labeled gelatin coated on the coverslips. As shown in Figures 4B and 4C, cells expressing Exo70-M displayed a high level of invadopodia activity. In contrast, cells expressing Exo70-E showed much lower invadopodia activity that was even weaker than that of the GFP control cells. Similar observations were made in MDA-MB-231 cells without endogenous Exo70 knockdown (Figure S3A) and MDA-MB-231 cells without Src overexpression (Figure S3B).

The exocyst complex is implicated in tumorigenesis, as its Sec5 and Exo84 subunits are direct downstream effectors of RalA and RalB, key components of the Ras signaling network (Balakireva et al., 2006; Bodemann et al., 2011; Issaq et al., 2010; Lim and Counter, 2005). We therefore also examined whether the Exo70 isoforms differentially affect tumorigenesis. Tumor cell proliferation was examined by generation of MDA-MB-231 cells with stable expression of Exo70-E or Exo70-M and measurement of the number of cells during 10 days of culturing. Cells with different Exo70 isoforms exhibited a similar growth rate (Figure 4E). Further examination of tumorigenesis by soft agar colony assay also showed no difference among these groups (Figure 4F). In fact, there is no detectable difference for Exo70-E and Exo70-M to interact with other exocyst components (discussed later). Our data suggest that Exo70-E and Exo70-M differ in mediating tumor invasion. The isoform switching of Exo70 may thus specifically affect cell motility rather than other aspects of exocyst function in cancer cells, including tumorigenesis.
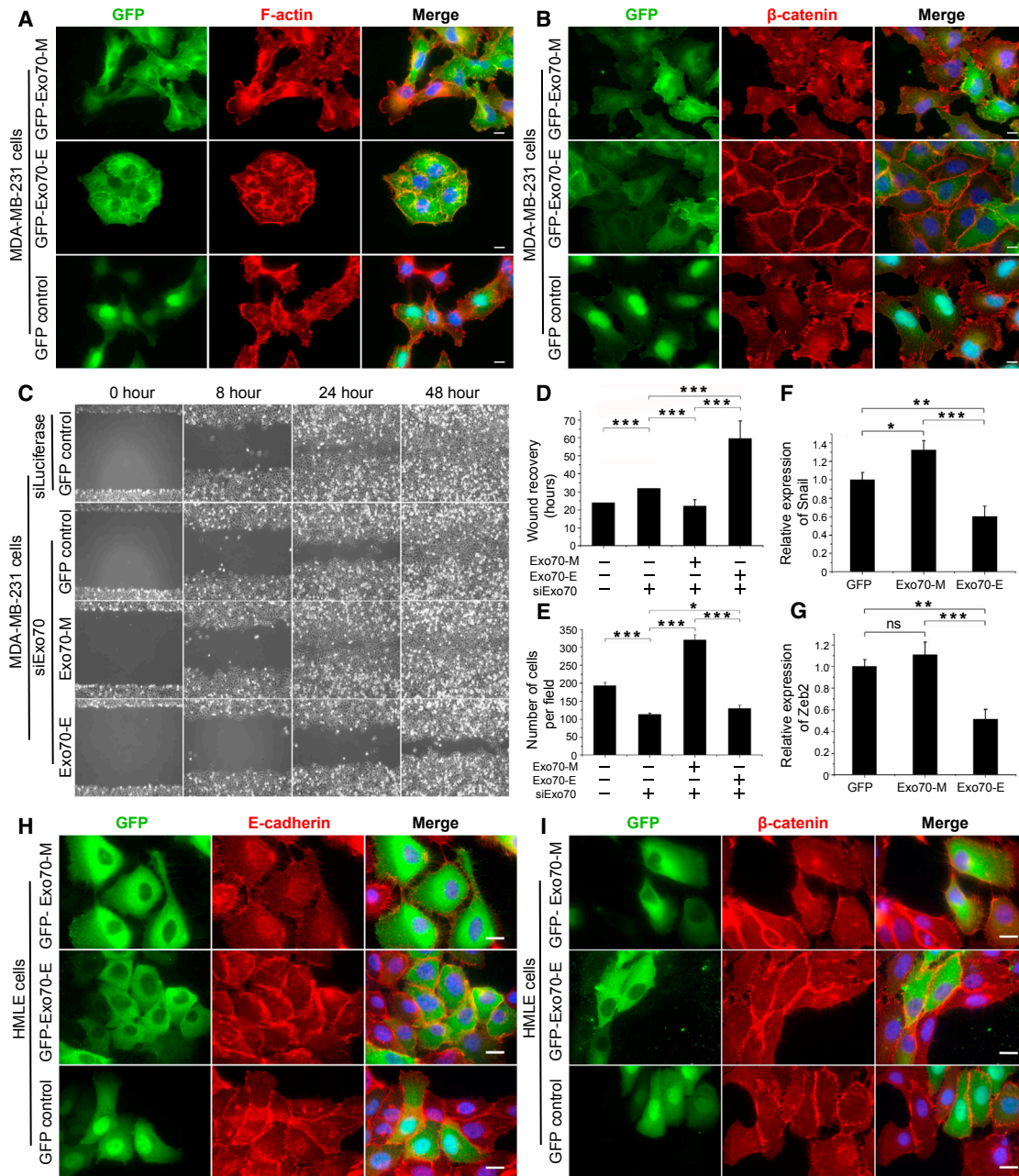
Figure 3. Expression of Specific Exo70 Isoforms Induces MET- or EMT-like Phenotypes

(A) Expression of Exo70-E in MDA-MB-231 cells induced epithelial-like cell phenotype. MDA-MB-231 cells stably expressing GFP-tagged Exo70-M or Exo70-E were fixed and stained for F-actin (red) and nucleus (blue). Expression of Exo70-E led to epithelial-like cell clustering, whereas cells expressing Exo70-M or GFP vector alone showed migratory phenotype as indicated by F-actin staining at the lamellipodia-like membrane expansions. At least three independent clones of stable cell lines were tested. Representative images are shown here. The same applies to the following experiments using stable cell lines. Scale bar, 10 μm

(B) Expression of GFP-Exo70-E, but not GFP-Exo70-M or GFP control, in MDA-MB-231 cells induced β-catenin relocalization to cell-cell contact sites. Scale bar, 10 μm.

(C) Wound healing assay of indicated MDA-MB-231 cell lines. The cells were imaged at 0, 8, 24, and 48 hr after the wounds were made.

(D) Quantification of wound healing assay. The MDA-MB-231 cells were imaged every 8 hr, and the time to complete wound closure was determined. n = 6. Three independent clones of stable cell lines were tested. ***p < 0.001.

(E) Transwell assays of MDA-MB-231 cell migration. Cells were imaged and counted 12 hr after being seeded in the chamber. n = 3, three independent replicates. *p < 0.05; ***p < 0.001.

(F and G) The mRNA levels of Snail (F) and ZEB2 (G) in MDA-MB-231 cells stably expressing GFP-tagged Exo70-M, Exo70-E, or GFP were detected by real-time PCR. Relative expression levels of Snail or Zeb2 in the cells expressing Exo70-M or Exo70-E were normalized to GFP control cells. n = 3. *p < 0.05; **p < 0.01; ***p < 0.001; ns, no statistic significance.

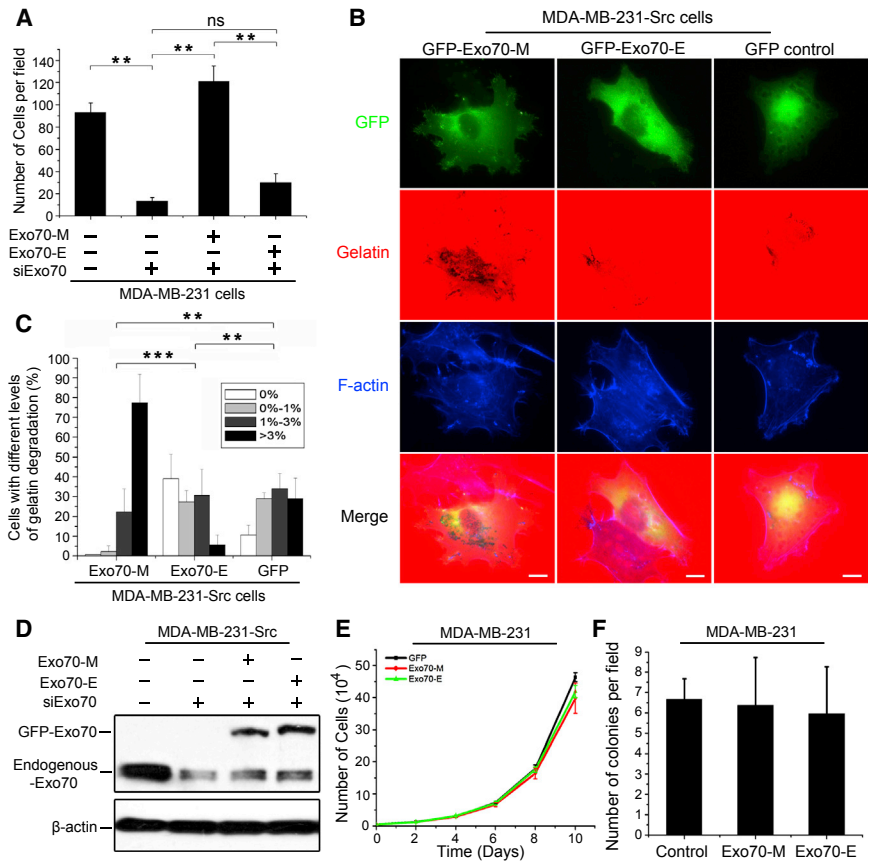*(legend continued on next page)*

Figure 4. Different Effects of Exo70 Isoforms on Invadopodia-Dependent ECM Degradation by MDA-MA-231 Cells

(A) Matrigel-transwell assays of MDA-MB-231 cell invasion. Cells with their endogenous Exo70 knocked down by RNAi were defective in invasion. Ectopic expression of Exo70-M rescued the invasion defects in Exo70 knockdown cells, whereas expression of Exo70-E in the cells was unable to restore cell invasiveness. Student's t test was performed using software R, version 2.14. n = 3, three independent replicates. **p < 0.01; ns, no statistic significance.

(B) MDA-MB-231-Src cells with their endogenous Exo70 knocked down by RNAi were transfected with GFP or GFP-Exo70 isoforms (green) and plated on coverslips coated with Alexa 568-labeled gelatin (red) for 8 hr. F-actin was detected by staining with Alexa-350-phalloidin (blue). Invadopodia activity was detected by the degradation of Alexa 568-labeled gelatin (shown as black holes). Comparing cells transfected with GFP alone, cells expressing Exo70-E had much reduced level of invasion (see cells with and without GFP-Exo70-E in the same field). In contrast, cells expressing Exo70-M had much increased levels of invasion. Scale bar, 10 μm.

(C) Percentage of cells with different levels of gelatin degradation was quantified. Three independent experiments were performed for each group, and 60 cells were counted for each group. An ANOVA was performed using software R, version 2.14. **p < 0.01; ***p < 0.001.

(D) The expression levels of GFP-Exo70 and endogenous Exo70 in the above siRNA-treated cells were examined by western blot. siRNA against luciferase was used as a control. The levels of β-actin were used as a loading control.

(E) Growth curves for Exo70-M and Exo70-E stable-expression cells. Cell numbers were counted every 2 days. ANOVA was performed using software R, version 2.14. Three independent replicates were performed for each group. p > 0.5.

(F) MDA-MB-231 cells stably expressing GFP-Exo70-M or GFP-Exo70-E or GFP control were cultured in soft agar. Number of colonies in nine fields was counted for each group. Student's t test was performed using software R, version 2.14. Three independent replicates were performed for each group. No differences among the three groups of cells were found.

Error bars indicate SD. See also Figure S3.

Expression of Different Exo70 Isoforms Does Not Affect MMP Secretion but Affects Actin-Mediated Protrusion during Invadopodia Formation

We next investigated the possible mechanisms that account for the ability of different Exo70 isoforms in invadopodia activity. First, we examined the exocytosis of matrix metalloproteinases (MMPs) mediated by Exo70 isoforms as Exo70 is part of the exocyst complex, which is known to regulate exocytosis, and was previously shown to mediate the secretion of MMP2 and MMP9. The levels of MMP secretion in cells expressing different Exo70 isoforms were compared by using the gelatin degradation zymography. As shown in Figures 5A and 5B, MDA-MB-231 cells with Exo70 knockdown had reduced levels of MMP2 and MMP9 secretion in the media; expression of either Exo70-E or Exo70-M rescued MMPs secretion in a similar fashion. Western blotting further confirmed that the expression of each isoform was at a similar level. We also compared the ability of Exo70-E and Exo70-M to interact with other exocyst components by coprecipitating experiments. MDA-MB-231 cells were transfected with glutathione S-transferase (GST)-tagged Exo70 isoforms, and then coprecipitation of endogenous Sec8, another exocyst component, from cells was examined. There was no difference in Sec8 binding to the two Exo70 isoforms (Figure 5C). Together, our data suggest that Exo70-E and Exo70-M do not differ in their ability to mediate exocytosis.

In addition to MMP secretion, effective ECM degradation by invadopodia at the invasion loci is also mediated by cell

(H) Immunofluorescence staining of E-cadherin (red) shows that E-cadherin localized to the plasma membrane in GFP control cells and cells expressing GFP-Exo70-E but was diffuse in the cytoplasm in cells expressing GFP-Exo70-M (green). Nuclei were stained with DAPI (blue). Scale bar, 10 μm.

(I) Immunofluorescence staining of β-catenin (red) shows their localization to the cell-cell contacts in control cells and cells expressing GFP-Exo70-E. In cells expressing GFP-Exo70-M (green), β-catenin was less associated with the plasma membrane. Nuclei were stained with DAPI (blue). Scale bar, 10 μm.

Student's t test was performed using software R, version 2.14. Error bars indicate SD. See also Figure S2.
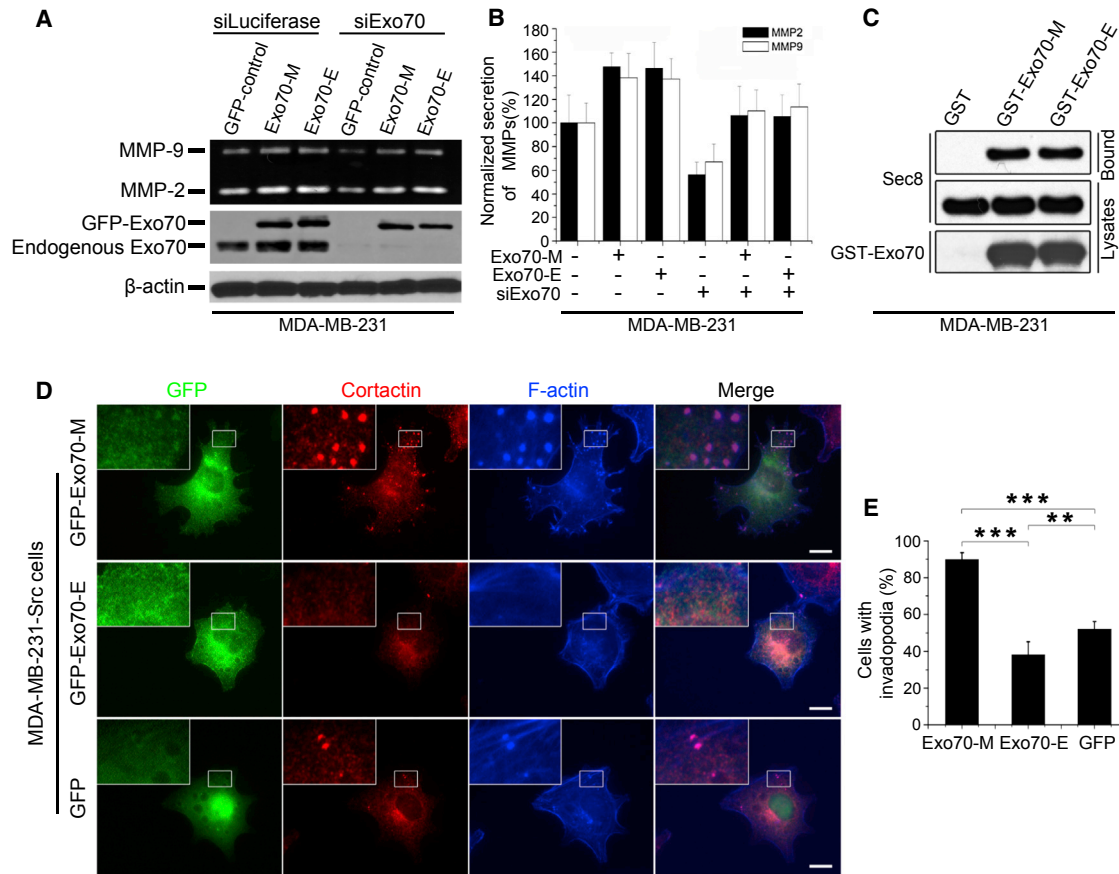
Figure 5. Expression of Specific Exo70 Isoforms Has No Effect on MMP Secretion but Has Significant Effect on Invadopodia Formation in MDA-MB-231 Cells

(A) In-gel zymography of MMP2 and MMP9 in MDA-MB-231 cells, MDA-MB-231 cells stably expressing siRNA-resistant GFP-Exo70-M or Exo70-E transfected with Exo70 siRNA or control siRNA. Expression levels of endogenous Exo70, exogenous GFP-Exo70, and β-actin were detected by western blot.

(B) Quantification of MMP secretion from different groups of cells (n = 3).

(C) Equal amounts of Sec8 were coprecipitated with GST-tagged Exo70-M and Exo70-E from MDA-MB-231 cell lysates.

(D) MDA-MB-231-Src cells with their endogenous Exo70 knocked down by RNAi were transfected with GFP or GFP-Exo70 isoforms (green) and plated on coverslips coated with 0.2% gelatin for 5 hr. Invadopodia were visualized by colocalization of cortactin (red) and F-actin (blue). Scale bar, 10 μm.

(E) Quantification of cells with invadopodia. Student's t test was performed using software R, version 2.14. n = 50 cells per sample, three independent replicates. **$p < 0.01$; ***$p < 0.001$.

Error bars indicate SD.

protrusions generated by actin polymerization beneath the plasma membrane (Pollard and Borisy, 2003; Ridley, 2011). It was thought that actin activity marks the initial stage of invadopodia formation, whereas MMP secretion occurs at the later mature stage of invadopodia activity (Murphy and Courtneidge, 2011). Actin organization in invadopodia can be studied by fluorescence localization of cortactin and F-actin (Bowden et al., 2006; Clark et al., 2007; Eckert et al., 2011; Oser et al., 2009). As shown in Figures 5D and 5E, while 52% of control MDA-MB-231-Src cells showed costaining of cortactin and F-actin, approximately 90% of cells exogenously expressing Exo70-M exhibited colocalized cortactin with F-actin staining. In contrast, cells exogenously expressing Exo70-E had reduced occurrence of cortactin and F-actin costaining at a level below that of the control cells. Taken together, our data suggest that Exo70-E and Exo70-M differ in their ability to promote actin dynamics, which contributes to their differences in invadopodia activities.

Exo70-M, but Not Exo70-E, Interacts with the Arp2/3 Complex and Stimulates Actin Branching

During cell invasion, the Arp2/3 complex generates a branched actin network that "pushes" the plasma membrane at the leading edges for cell migration and invasion (Goley and Welch, 2006; Insall and Machesky, 2009; Pollard and Borisy, 2003; Ridley, 2011). In invadopodia, the Arp2/3 complex plays an essential role in protrusion formation (Gimona et al., 2008; Murphy and Courtneidge, 2011; Nürnberg et al., 2011; Weaver, 2006; Yamaguchi et al., 2005). Having determined that the splicing of Exo70 isoforms did not affect MMP secretion, we next investigated whether the Exo70 isoforms differentially affect the Arp2/3 complex, as we had previously found that rat Exo70 can bind to the Arpc1 subunit of Arp2/3 complex and is involved in invadopodia formation (Liu et al., 2009; Ren and Guo, 2012; Zuo et al., 2006). Using recombinant Exo70 and Arpc1, we found that a substantially greater amount of Arpc1 bound to Exo70-M compared to

Exo70-E (Figure 6A). Similarly, in MDA-MB-231 cells expressing GST-Exo70 and myc-Arpc1, Exo70-M, but not Exo70-E, bound to Arpc1 (Figure 6B). Furthermore, Exo70-M was able to bind to the purified Arp2/3 complex more strongly than Exo70-E (Figures S5F and S5G).

The Arp2/3 complex, upon activation by the N-WASP/WAVE family of proteins, generates new actin filaments on the side of preexisting filaments at a 70° angle. The in vitro generation of actin branches can be monitored in real time using total internal reflection fluorescence (TIRF) microscopy (Amann and Pollard, 2001a, 2001b). Here, we determined the effect of Exo70-E and Exo70-M on the Arp2/3 complex-mediated actin branching using dual-color time-lapse TIRF microscopy. Rhodamine-labeled G-actin was polymerized for 3 min and immobilized on a NEM-myosin-coated glass slide. Cy5-labeled G-actin with protein mixtures containing the purified Arp2/3 complex and WAVE2 together with purified Exo70-M or Exo70-E were flowed into the chamber to replace the free rhodamine-labeled G-actin. The generation of new filamentous actin was monitored over time. As shown in Figure 6C, addition of Exo70-M substantially stimulated actin branching mediated by the Arp2/3 complex and WAVE2 (see also Movie S1 for better audio and visual presentations of the generations of nascent actin branches). On the other hand, Exo70-E did not have a significant effect. Quantification of actin branch generation ("branching ratio": branches per preexisting actin filament) over time is shown in Figure 6D.

We have previously generated an Exo70-M mutant, Exo70-M(Δ628-630), which is specifically defective in binding to the Arp2/3 complex (Liu et al., 2012; Zuo et al., 2006). We found that MDA-MB-231 cells expressing Exo70-M, but not Exo70-E or Exo70-M(Δ628-630), show recruitment of the Arp2/3 complex to the leading edge (Figure S4A). Furthermore, similar to Exo70-E, stable expression of Exo70-M(Δ628-630) in MDA-MB-231 cells induced a more epithelial-like morphology (Figure 6E). Expression of Exo70-M(Δ628-630) in MDA-MB-231 cells with their endogenous Exo70 knocked down inhibited cell migration, cell invasion, and invadopodia formation in the transwell assay and gelatin degradation assay (Figures 6F, 6G, S5A, and S5B). Moreover, we found that expression of Exo70-M(Δ628-630) failed to induce E-cadherin and β-catenin relocalization in HMLE cells (Figures S4B and S4C). Interestingly, expression of Exo70-M(Δ628-630) decreased expression of Snail and Zeb2 (Figure S5C), which is similar to the increased expression of Exo70-E in cells. These data suggest that the capability of Exo70-M to promote cell invasion rely on its interaction with the Arp2/3 complex.

Exo70-E and Exo70-M Have Opposite Effects on Tumor Metastasis in Mice

To determine whether the differences in Exo70 isoform expression at the cellular level are pathologically relevant, we subcutaneously inoculated MDA-MB-231 cells stably expressing different Exo70 isoforms in immunodeficient mice. Tumor metastasis in these mice was monitored over a period of 5 weeks. While tumor incidence was similar for each group (Figure 7A), Exo70-E expression was found to efficiently suppress lung metastasis (Figures 7B and 7C). The tumor tissues were also stained for cortactin, which was used as a marker of dynamic actin activity (Clark et al., 2007; Eckert et al., 2011; Oser et al., 2009). Tumor

tissues expressing GFP-Exo70-E had a much lower level of cortactin foci staining compared to those expressing GFP alone, whereas tumor tissues expressing GFP-Exo70-M had a much higher level of cortactin foci (Figures S6A and S6B).

Exo70 Isoforms Are Differentially Expressed in Human Breast Tumors

The results presented earlier suggest a link between Exo70 isoform switching and tumor invasion and, thus, led us to test whether the expression of these Exo70 isoforms correlates with tumor progression in human tissue. Examination of Exo70-E and Exo70-M splicing variant mRNA expression in human breast tumor tissues revealed that the ratio of Exo70-E to Exo70-M (the E/M ratio) was significantly lower in patients in which the tumor had invaded the lymph nodes compared to samples in which the tumor remained localized (p < 0.001; Figures 7D and 7E). Furthermore, quantitative PCR (qPCR) analysis of the mRNA levels of ESRP1 in the tumor samples demonstrated a positive correlation between ESRP1 mRNA expression and E/M ratio (p < 0.05; Figure 7F). These findings suggest that Exo70 isoform switching is likely regulated by ESRP in breast tumor tissue.

DISCUSSION

While the role of transcriptional regulation in EMT has been well established (Thiery et al., 2009; Yang et al., 2006), alternative splicing has recently emerged as an important modulator of EMT (Lapuk et al., 2010; Shapiro et al., 2011; Warzecha and Carstens, 2012). ESRP1 and ESRP2 were identified as important splicing factors (Dittmar et al., 2012; Warzecha et al., 2009, 2010) that mediate the expression of different isoforms of proteins such as FGFR2, p120 catenin, CD44, and Mena, that participate in polarity establishment, adherens junction formation, and actin cytoskeleton reorganization (Brown et al., 2011; Goswami et al., 2009; Lipski et al., 2008; Ohkubo and Ozawa, 2004; Savagner et al., 1994). The data presented in this study demonstrate that the Exo70 subunit of the exocyst complex has splicing isoforms that are differentially expressed during EMT. Expression of Exo70-E in mesenchymal cells induced cell–cell contact and attenuated cell motility, whereas expression of Exo70-M promoted invadopodia formation and cell invasion. The current study demonstrates that isoform switching of Exo70 plays an important role in the transition between the epithelial and mesenchymal states.

ESRP1 and ESRP2 govern the pre-mRNA processing activities of an array of genes, and a loss of ESRP expression induces some of the cellular changes that occur in EMT (Warzecha et al., 2010), suggesting that global shifts in transcript variants may potently drive EMT program. This is, to some extent, similar to the global changes in gene expression levels induced by transcription factors. For example, Snail has been reported to be able to promote the splicing of p120 catenin, leading to enhanced expression of mesenchymal p120 catenin isoform (Ohkubo and Ozawa, 2004; Yanagisawa et al., 2008). These data suggest that some cross-communication exists between alternative splicing and transcriptional regulation. In the current study, we found that increased expression of Exo70-E led to a decrease of Snail and ZEB2 expression, which results in transcriptional changes of their target genes and, therefore,
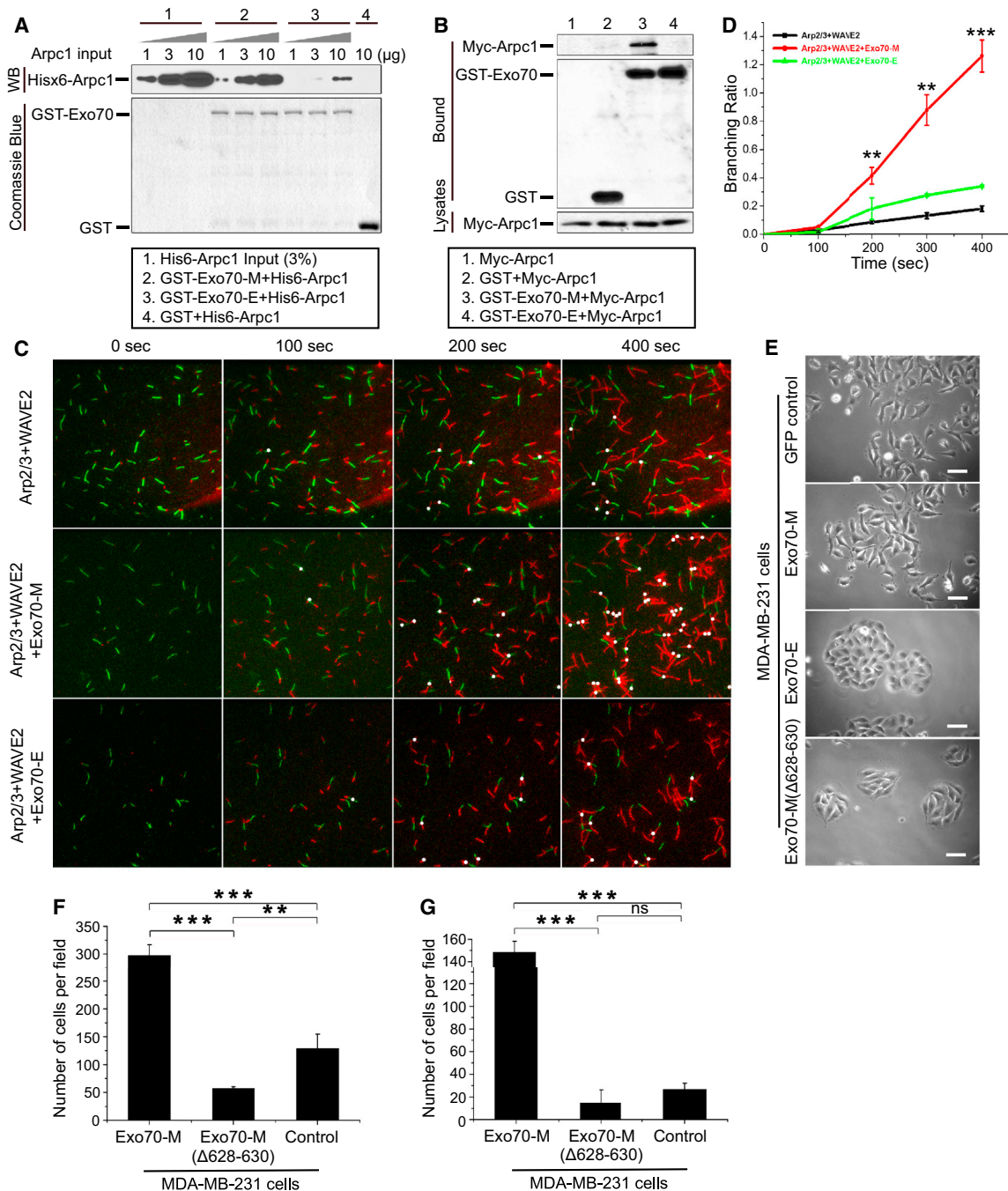
Figure 6. Exo70-M, but Not Exo70-E, Interacts with the Arp2/3 Complex and Stimulates Actin Branching

(A) In vitro binding of GST-Exo70-E and Exo70-M with Hisx6-Arpc1. GST-Exo70 isoforms were immobilized on glutathione-Sepharose and then incubated with 1 μg, 3 μg, or 10 μg of Hisx6-Arpc1, respectively. Input and bound Hisx6-Arpc1 were analyzed by western blot with anti-Hisx6 antibody. GST and GST-tagged Exo70 isoforms are stained with Coomassie blue. GST-Exo70-M showed strong dose-dependent interactions with Hisx6-Arpc1.

(B) The binding of Exo70-M and Arpc1 in cells. GST-Exo70-E, GST-Exo70-M, and GST were cotransfected with Myc-Arpc1 into MDA-MB-231 cells. Arpc1 coprecipitated with Exo70-M but not Exo70-E.

(C) Exo70-M, but not Exo70-E, stimulated the Arp2/3 complex-mediated actin branching as observed by dual-color time-lapse TIRF microscopy. After 2 μM of 6% rhodamine-labeled G-actin (green) had been allowed to polymerize in the flow chamber for 3 min, 0.8 μM of 8% Cy5-labeled actin (red) with all the proteins was loaded into the chamber to replace the rhodamine-labeled actin. Frames are shown at 0, 100, 200, and 400 s after the Cy5-G-actin and protein mixture had been loaded. The newly generated branches are indicated by white dots.

(D) Quantification of actin branching over time. Branching ratio was defined as the number of branches divided by the number of total actin filaments in the same field. n = 3. **p < 0.01; ***p < 0.001.

(E) Expression of Exo70-M(Δ628-630) in MDA-MB-231 cells induced epithelia-like morphology. Scale bar, 50 μm.
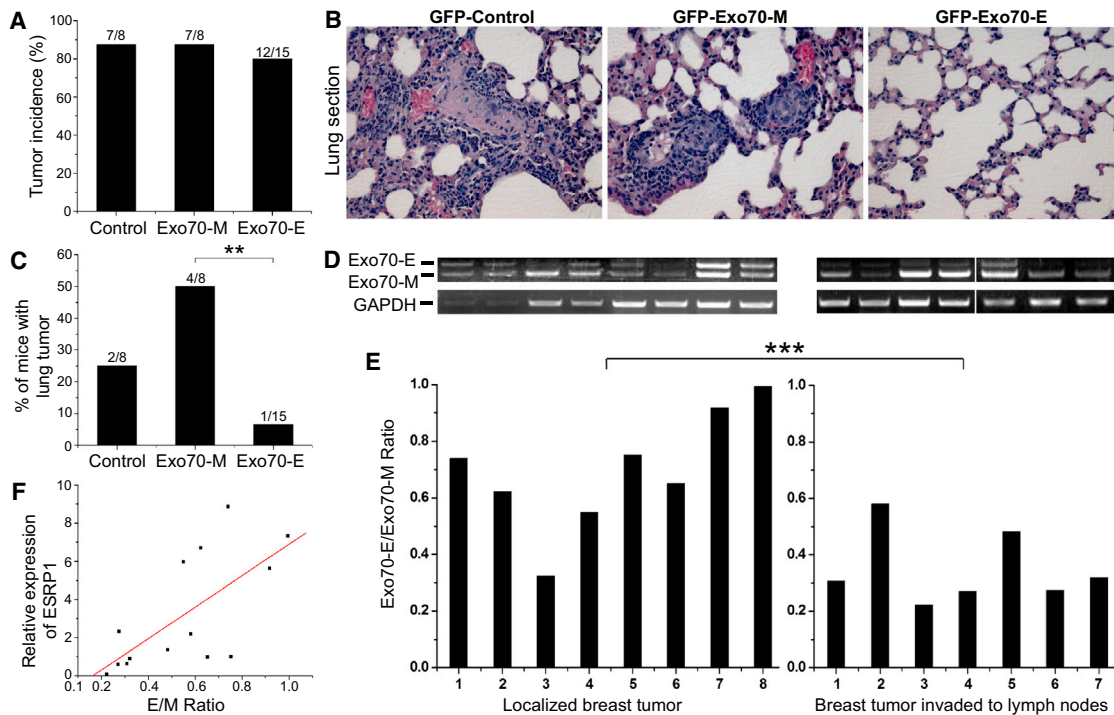
(legend continued on next page)

Figure 7. Different Effects of Exo70 Isoforms on Tumor Metastasis

(A) Tumor incidence 5 weeks after introducing MDA-MB-231 cells stably expressing Exo70-E, Exo70-M, or GFP to immunodeficient mice.

(B) Representative images of hematoxylin and eosin staining of mice lung sections.

(C) Percentage of mice with lung tumors among the three different groups of mice.

(D) RT-PCR analysis of Exo70-E and Exo70-M expression in patient breast tumors. The left panel shows tumor samples collected from patients with localized breast tumors. The right panel shows tumor samples collected from patients with breast tumors invaded to lymph nodes. Note that the total amounts of RNA collected from these clinical samples were different as indicated by GAPDH levels.

(E) The Exo70-E to Exo70-M ratio of each sample in (D) is calculated with ImageJ software. ***p < 0.001. ANOVA was performed using software R, version 2.14.

(F) Ratio of Exo70-E to Exo70-M mRNA level (the E/M ratio) in each tumor sample plotted against the corresponding ESRP1 mRNA level in the same sample. Linear regression analysis was performed using software R, version 2.14; p < 0.05.

See also Figure S6.

attenuation of EMT. This result raises the possibility that targets of ESRP splicing also, in turn, modulate the transcription program of EMT, thus adding another layer of complexity to the regulatory network of EMT. Future biochemical and cell biological analyses, together with multifactor simulation using systems biology, may help elucidate the interplays among these regulatory paradigms.

From the perspective of cell morphology, a shift from the apical-basolateral polarity to "front-rear" polarity takes place during EMT. The exocyst complex has been localized to adherens junctions and mediates the establishment of epithelial polarity (Grindstaff et al., 1998; Nelson, 2003; Yeaman et al., 2004). In addition, the exocyst has been observed to mediate the incorporation of E-cadherin to the plasma membrane for the establishment and maintenance of cell-cell junction (Langevin et al., 2005; Leibfried et al., 2008). Therefore, the exocyst

plays an important role in epithelial polarity. On the other hand, the exocyst, especially the Exo70 subunit, has also been shown to mediate directional cell migration (Letinic et al., 2009; Liu et al., 2009; Rosse et al., 2009; Rossé et al., 2006; Thapa et al., 2012; Zuo et al., 2006). Here, we show that Exo70-M, but not Exo70-E, interacts with, and kinetically stimulates, the Arp2/3 complex to promote branched actin network formation, which is essential for the generation of membrane protrusions such as invadopodia. Our work thus provides a possible mechanism for the observed switch in cellular phenotypes. It also demonstrates that alternative splicing of an evolutionarily conserved "housekeeping" gene can account for two seemingly paradoxical behaviors. Exo70-E differs from Exo70-M by a 23-amino-acid insertion conferred by ESRP splicing. It is possible that this insertion leads to conformational changes of the Exo70 protein that negatively affect its interaction with the Arp2/3 complex. It is

(F) Transwell assay of MDA-MB-231 cells with their endogenous Exo70 knocked down by RNAi were defective in migration. Ectopic expression of Exo70-M(Δ628-630) was unable to rescue the migration defects in Exo70 knockdown cells. n = 3. **p < 0.01; ***p < 0.001.

(G) Matrigel-transwell assay shows that MDA-MB-231 cells with their endogenous Exo70 knocked down by RNAi were defective in invasion. Ectopic expression of Exo70-M(Δ628-630) was unable to rescue the invasion defects in Exo70 knockdown cells. n = 3. ***p < 0.001; ns, no statistical significance.

Student's t test was performed using software R, version 2.14. Error bars indicate SD. See also Figures S4, S5, and Movie S1.

interesting to note that land plants have around 20 Exo70 paralogs per genome; this diversification during evolution is thought to be related to the diverse structures of the endomembranes and surface domains observed in land plants and their competition with parasites (Cvrčková et al., 2012; Zárský et al., 2009).

In addition to tumor invasion, the exocyst complex has previously been demonstrated to play a role in tumorigenesis. Two of the exocyst subunits, Sec5 and Exo84, directly interact with the guanosine triphosphate (GTP)-bound form of RalA and RalB, which are components of the Ras signaling pathway (Balakireva et al., 2006; Bodemann et al., 2011; Camonis and White, 2005; Feig, 2003; Issaq et al., 2010; Lim and Counter, 2005; Moskalenko et al., 2002; Moskalenko et al., 2003; Polzin et al., 2002). The Ral-exocyst interaction is required for the subsequent activation of oncogenic kinases such as TBK1 (Balakireva et al., 2006; Bodemann et al., 2011). Our data suggest that different Exo70 isoforms have the same interactions with the other exocyst components. The isoform switching of Exo70 does not affect the function of the exocyst complex in exocytosis and oncogenesis but rather serves as a regulatory mechanism that controls EMT and tumor metastasis. Together, these studies suggest that the exocyst complex is implicated in several key stages of cancer and may provide a link between tumorigenesis and cancer dissemination. Future studies of Exo70 and the exocyst complex may hold exciting potentials for diagnosis and therapeutics of cancer.

EXPERIMENTAL PROCEDURES

Plasmids and antibodies, RNA extraction, RT-PCR, real-time PCR, and immunofluorescence assay are described in the Supplemental Experimental Procedures.

Cell Culture and Transfection

The study protocol that uses human cells was approved by the institutional review board of the University of Pennsylvania. MDA-MB-231 and MCF7 cells were cultured in Dulbecco's modified Eagle's medium (DMEM) (Invitrogen) supplemented with 10% fetal bovine serum (FBS), 2 mM of L-glutamine, 100 U/ml of penicillin, and 100 of μg/ml streptomycin. Maintenance of the immortalized HMLE and HMLE/Twist-ER cells was performed as described (Yang et al., 2004). DNA transfection into cells was conducted using LipofectAMINE 2000 (Invitrogen) or Fugene 6 (Roche), and RNA transfection into cells was conducted using LipofectAMINE RNAiMAX (Invitrogen). The Human Exo70 siRNA target sequence was 5′- GGTTAAAGGTGACTGATTA-3′ and the control Luciferase GL2 siRNA target sequence was 5′- AACGTACGCG GAATACTTCGA-3′. Cells were harvested 48 hr after transfection.

Stable MDA-MB-231 cell lines expressing GFP, GFP-Exo70-E, and GFP-Exo70-M were selected using G418 (1 mg/ml). Single positive colonies were selected by fluorescence-activated cell sorting (FACS; Flow Cytometry and Cell Sorting Resource Laboratory, University of Pennsylvania). Colonies were maintained in DMEM for 2 weeks, and multiple clones were isolated and used for subsequent experiments. Expression levels were determined by fluorescence microscopy and western blotting. Cluster formation was observed in MDA-MB-231 cells by seeding them at 2×10^3 cells per well in a six-well dish. Cells were maintained in DMEM for 1–2 weeks before microscopy.

Binding Experiments

For Hisx6-Arpc1 and GST-Exo70 binding assay, Hisx6-Arpc1 and GST-Exo70 were purified from bacteria. A total of 5 μg of GST-Exo70-E or GST-Exo70-M and 1 μg, 3 μg, or 10 μg of His-Arpc1 were diluted in 0.6 ml of binding buffer (20 mM of HEPES, pH 7.4; 1 mM of EDTA; 150 mM of NaCl; 1% Triton X-100; 1 mM of dithiothreitol (DTT); and protease inhibitors cocktail), and mixed with 30 μl (50% v/v) of glutathione Sepharose-4B. After overnight incu-

bation at 4°C, beads were washed five times with the same binding buffer, and the bound proteins were analyzed by western blotting.

To detect the interaction of Arpc1 with Exo70 in cells, MDA-MB-231 cells were cotransfected with Myc-Arpc1 and GST-Exo70-E, GST-Exo70-M, or GST vector. Cells were harvested at 72 hr posttransfection and lysed in the lysis buffer (20 mM of HEPES, pH 7.4; 1 mM of EDTA; 150 mM of NaCl; 0.5% Triton X-100; 1 mM of DTT, and protease inhibitors). After cell lysates were incubated overnight with glutathione Sepharose-4B at 4°C, the beads were washed five times with the lysis buffer, and the bound proteins were analyzed by western blotting using an anti-Myc monoclonal antibody.

To examine the interaction between the Exo70 isoforms and the Arp2/3 complex, we purified GST-Exo70 isoforms from bacteria. The GST tag on Exo70 isoforms were removed by PreScission Protease. Arp2/3 complex was purified as described previously (Liu et al., 2012). For the binding reaction, 1 μg Exo70, 1 μg GST-CA protein, and 5 μg of Arp2/3 complex were diluted in 0.6 ml of binding buffer, described earlier, and mixed with 20 μl (50% v/v) of glutathione Sepharose-4B beads. After overnight incubation at 4°C, the beads were washed five times with the same binding buffer, and the bound proteins were analyzed by western blotting.

Wound Healing Assay and Transwell Assay

For wound healing assay, cells were cultured to confluence on 6-well plates, and a scratch was made using a pipette tip. Cells were washed with PBS to remove the detached cells and the remaining cells were incubated with regular medium and observed every 8 hr until the time point of complete wound closure. Assays were repeated three times for each clone.

The transwell migration assay was performed by seeding 1×10^5 MDA-MB-231 cells that had undergone different treatments to the upper chamber of transwell inserts (6.5 mm in diameter with 8.0-μm pores, Corning). Serum-free DMEM was added to the cells in the upper chamber and 700 μl of DMEM containing 10% FBS to the lower chamber. After 12 hr of incubation, the inserts were washed with PBS, and the migrated cells on the lower side of the membrane were fixed and stained with Giemsa stain. The number of cells was counted in three randomly chosen fields per transwell insert. For the Matrigel-transwell assay, the procedure was similar with the transwell migration assay, except that the transwell membranes were precoated with 40 ng of Matrigel (BD Biosciences), and the cells were incubated for 24 hr.

Soft Agar Assay for Colony Formation

MDA-MB-231 cells stably expressing GFP, GFP-Exo70-E, or Exo70-M were seeded in six-well plates at a density of 500 cells per well. Each well contained 1 ml of 0.7% soft agar in complete DMEM as the bottom layer and 1 ml of 0.38% agar in complete DMEM as the feeder layer. After 3 weeks of incubation, the number of colonies was determined under microscopy at 100× magnification, with three independent wells examined for each group.

Monitoring Actin Branching using TIRF Microscopy

TIRF microscopy analysis of actin branching was performed as described previously (Amann and Pollard, 2001b). Briefly, after glass coverslips and Dow Corning 732 multipurpose silicone sealant had been used to prepare chambers, 50 nM of N-ethyl maleimide (NEM)-myosin in high salt buffer (500 mM of KCl) was used to immobilize actin filaments and 1% BSA was used to block nonspecific binding to the surface. Proteins were mixed in the actin polymerization buffer (60 mM of KC1; 2.5 mM of NaCl; 0.6 mM of $MgCl_2$; 5 mM of Tris-HCl, pH 7.5; 2.5 mM of HEPES, pH 7.1; 0.5 mM of EGTA; 30 μM of $CaCl_2$; 0.2 mM of ATP; and 0.3 mM of NaN_3) and incubated for 30 min at 4°C. After 2 μM of Mg^{2+}-G-actin (6% rhodamine labeled) in polymerization buffer had been loaded into the flow chamber and allowed to polymerize for 3 min, it was replaced with 0.8 μM of Mg^{2+}-G-actin (8% Cy5 labeled) and a protein mixture (15 nM of Arp2/3 complex, 25 nM of WAVE2, and 250 nM of Exo70-M or Exo70-E) in polymerization buffer. Immediately after the addition of Cy5-labeled actin, the chamber was imaged every 2 s by TIRF microscopy for 10 min (Nikon TE2000U inverted microscope with an in-house TIRF illuminator).

In-Gel Zymography

In-gel zymography assay was performed for detection of MMP secretion as described previously (Liu et al., 2009). After cells had been cultured in

Cell
PRESS

serum-free DMEM for 24 hr, the media were collected and concentrated. Samples were then separated on 8% polyacrylamide/0.3% gelatin gel. Following electrophoresis, the gel was washed twice in 2.5% Triton X-100 and incubated in reaction buffer (50 mM of Tris-HCl, pH 8.0, and 5 mM of CaCl$_2$) at 37°C for 24 to 48 hr. After the reaction, the gel was stained with staining buffer (0.12% Coomassie blue R-250, 50% methanol, and 20% acetic acid) for 1 hr and destained overnight with destaining buffer (22% methanol and 10% acetic acid). Gel loading values were normalized to total protein measured using a Bio-Rad Protein Assay Kit, with measurement of each sample repeated three times.

In Situ Zymography

The protocol used to perform in situ zymography was adapted from the Mueller Laboratory (Artym et al., 2009). In brief, Alexa Fluor 568-conjugated gelatin was prepared by Alexa Fluor 568 protein labeling (Molecular Probes) according to the manufacturer's instructions. After 18-mm coverslips had been incubated in 20% nitric acid for 30 min and washed with water, they were incubated with 50 μg/ml of poly-L-lysine (Sigma) for 20 min, fixed with 0.5% glutaraldehyde (Ted Pella) for 15 min, and washed with PBS. The coverslips were then inverted onto 60-μl droplets of gelatin matrix (0.2% gelatin and Alexa Fluor 568-labeled gelatin at an 8:1 ratio) for 10 min, washed in PBS, and incubated in 5 mg/ml of NaBH$_4$ for 15 min. After the coverslips had been washed in PBS and incubated in DMEM for 2 hr, 2 × 10^4 cells were seeded on to the coverslips and incubated at 37°C for 8 hr, and then processed for immunofluorescence. Each experiment was repeated three times. Gelatin degradation was quantified using ImageJ software, with the degradation level of each cell measured as the area of the degraded zones per cell relative to the area of the entire cell. For quantification of gel degradation, the percentage of cells with different degradation levels was calculated.

Xenograft Tumor Model

A xenograft tumor model was created by subcutaneous injection of MDA-MB-231 cells (2 × 106 cells per animal) stably expressing GFP, Exo70-E, or Exo70-M into 8, 8, and 15, respectively, 4- to 5-week-old female athymic nu/nu mice. Tumors were palpable at approximately 1 week, and caliper measurements were obtained twice per week. Mice were sacrificed after 5 weeks. Lungs were harvested and embedded in paraffin, sectioned, stained with hematoxylin and eosin, and then imaged. Lungs with tumor were identified as an indicator of metastasis. Mice with lung tumor were counted and statistics analysis (Fisher's exact test) was performed. The animal research was approved by the Institutional Animal Care and Use Committee at the University of Pennsylvania.

Statistical Analyses

All statistical analyses (Student's t test, ANOVA, and linear regression analysis) were performed using software R, version 2.14.

SUPPLEMENTAL INFORMATION

Supplemental Information includes Supplemental Experimental Procedures, six figures, one table, and one movie and can be found with this article online at http://dx.doi.org/10.1016/j.devcel.2013.10.020.

REFERENCES

Amann, K.J., and Pollard, T.D. (2001a). The Arp2/3 complex nucleates actin filament branches from the sides of pre-existing filaments. Nat. Cell Biol. 3, 306–310.

Amann, K.J., and Pollard, T.D. (2001b). Direct real-time observation of actin filament branching mediated by Arp2/3 complex using total internal reflection fluorescence microscopy. Proc. Natl. Acad. Sci. USA 98, 15009–15013.

Artym, V.V., Yamada, K.M., and Mueller, S.C. (2009). ECM degradation assays for analyzing local cell invasion. Methods Mol. Biol. 522, 211–219.

Balakireva, M., Rossé, C., Langevin, J., Chien, Y.C., Gho, M., Gonzy-Treboul, G., Voegeling-Lemaire, S., Aresta, S., Lepesant, J.A., Bellaiche, Y., et al. (2006). The Ral/exocyst effector complex counters c-Jun N-terminal kinase-dependent apoptosis in Drosophila melanogaster. Mol. Cell. Biol. 26, 8953–8963.

Bodemann, B.O., Orvedahl, A., Cheng, T., Ram, R.R., Ou, Y.H., Formstecher, E., Maiti, M., Hazelett, C.C., Wauson, E.M., Balakireva, M., et al. (2011). RalB and the exocyst mediate the cellular starvation response by direct activation of autophagosome assembly. Cell 144, 253–267.

Bowden, E.T., Onikoyi, E., Slack, R., Myoui, A., Yoneda, T., Yamada, K.M., and Mueller, S.C. (2006). Co-localization of cortactin and phosphotyrosine identifies active invadopodia in human breast cancer cells. Exp. Cell Res. 312, 1240–1253.

Brown, R.L., Reinke, L.M., Damerow, M.S., Perez, D., Chodosh, L.A., Yang, J., and Cheng, C. (2011). CD44 splice isoform switching in human and mouse epithelium is essential for epithelial-mesenchymal transition and breast cancer progression. J. Clin. Invest. 121, 1064–1074.

Bryant, D.M., Datta, A., Rodríguez-Fraticelli, A.E., Peränen, J., Martín-Belmonte, F., and Mostov, K.E. (2010). A molecular network for de novo generation of the apical surface and lumen. Nat. Cell Biol. 12, 1035–1045.

Camonis, J.H., and White, M.A. (2005). Ral GTPases: corrupting the exocyst in cancer cells. Trends Cell Biol. 15, 327–332.

Clark, E.S., Whigham, A.S., Yarbrough, W.G., and Weaver, A.M. (2007). Cortactin is an essential regulator of matrix metalloproteinase secretion and extracellular matrix degradation in invadopodia. Cancer Res. 67, 4227–4235.

Cvrčková, F., Grunt, M., Bezvoda, R., Hála, M., Kulich, I., Rawat, A., and Žárský, V. (2012). Evolution of the land plant exocyst complexes. Front. Plant Sci. 3, 159.

Dittmar, K.A., Jiang, P., Park, J.W., Amirikian, K., Wan, J., Shen, S., Xing, Y., and Carstens, R.P. (2012). Genome-wide determination of a broad ESRP-regulated posttranscriptional network by high-throughput sequencing. Mol. Cell. Biol. 32, 1468–1482.

Eckert, M.A., Lwin, T.M., Chang, A.T., Kim, J., Danis, E., Ohno-Machado, L., and Yang, J. (2011). Twist1-induced invadopodia formation promotes tumor metastasis. Cancer Cell 19, 372–386.

Feig, L.A. (2003). Ral-GTPases: approaching their 15 minutes of fame. Trends Cell Biol. 13, 419–425.

Feltes, C.M., Kudo, A., Blaschuk, O., and Byers, S.W. (2002). An alternatively spliced cadherin-11 enhances human breast cancer cell invasion. Cancer Res. 62, 6688–6697.

Gimona, M., Buccione, R., Courtneidge, S.A., and Linder, S. (2008). Assembly and biological role of podosomes and invadopodia. Curr. Opin. Cell Biol. 20, 235–241.

Goley, E.D., and Welch, M.D. (2006). The ARP2/3 complex: an actin nucleator comes of age. Nat. Rev. Mol. Cell Biol. 7, 713–726.

Goswami, S., Philippar, U., Sun, D., Patsialou, A., Avraham, J., Wang, W., Di Modugno, F., Nistico, P., Gertler, F.B., and Condeelis, J.S. (2009). Identification of invasion specific splice variants of the cytoskeletal protein Mena present in mammary tumor cells during invasion in vivo. Clin. Exp. Metastasis 26, 153–159.

Grindstaff, K.K., Yeaman, C., Anandasabapathy, N., Hsu, S.C., Rodriguez-Boulan, E., Scheller, R.H., and Nelson, W.J. (1998). Sec6/8 complex is recruited to cell-cell contacts and specifies transport vesicle delivery to the basal-lateral membrane in epithelial cells. Cell 93, 731–740.

He, B., and Guo, W. (2009). The exocyst complex in polarized exocytosis. Curr. Opin. Cell Biol. *21*, 537–542.

Hsu, S.C., TerBush, D., Abraham, M., and Guo, W. (2004). The exocyst complex in polarized exocytosis. Int. Rev. Cytol. *233*, 243–265.

Huber, M.A., Kraut, N., and Beug, H. (2005). Molecular requirements for epithelial-mesenchymal transition during tumor progression. Curr. Opin. Cell Biol. *17*, 548–558.

Insall, R.H., and Machesky, L.M. (2009). Actin dynamics at the leading edge: from simple machinery to complex networks. Dev. Cell *17*, 310–322.

Issaq, S.H., Lim, K.H., and Counter, C.M. (2010). Sec5 and Exo84 foster oncogenic ras-mediated tumorigenesis. Mol. Cancer Res. *8*, 223–231.

Langevin, J., Morgan, M.J., Sibarita, J.B., Aresta, S., Murthy, M., Schwarz, T., Camonis, J., and Bellaïche, Y. (2005). Drosophila exocyst components Sec5, Sec6, and Sec15 regulate DE-Cadherin trafficking from recycling endosomes to the plasma membrane. Dev. Cell *9*, 365–376.

Lapuk, A., Marr, H., Jakkula, L., Pedro, H., Bhattacharya, S., Purdom, E., Hu, Z., Simpson, K., Pachter, L., Durinck, S., et al. (2010). Exon-level microarray analyses identify alternative splicing programs in breast cancer. Mol. Cancer Res. *8*, 961–974.

Leibfried, A., Fricke, R., Morgan, M.J., Bogdan, S., and Bellaiche, Y. (2008). Drosophila Cip4 and WASp define a branch of the Cdc42-Par6-aPKC pathway regulating E-cadherin endocytosis. Current biology: CB *18*, 1639–1648.

Letinic, K., Sebastian, R., Toomre, D., and Rakic, P. (2009). Exocyst is involved in polarized cell migration and cerebral cortical development. Proc. Natl. Acad. Sci. USA *106*, 11342–11347.

Lim, K.H., and Counter, C.M. (2005). Reduction in the requirement of oncogenic Ras signaling to activation of PI3K/AKT pathway during tumor maintenance. Cancer Cell *8*, 381–392.

Linder, S. (2007). The matrix corroded: podosomes and invadopodia in extracellular matrix degradation. Trends Cell Biol. *17*, 107–117.

Lipski, A.M., Pino, C.J., Haselton, F.R., Chen, I.W., and Shastri, V.P. (2008). The effect of silica nanoparticle-modified surfaces on cell morphology, cytoskeletal organization and function. Biomaterials *29*, 3836–3846.

Liu, J., and Guo, W. (2012). The exocyst complex in exocytosis and cell migration. Protoplasma *249*, 587–597.

Liu, J., Zuo, X., Yue, P., and Guo, W. (2007). Phosphatidylinositol 4,5-bisphosphate mediates the targeting of the exocyst to the plasma membrane for exocytosis in mammalian cells. Mol. Biol. Cell *18*, 4483–4492.

Liu, J., Yue, P., Artym, V.V., Mueller, S.C., and Guo, W. (2009). The role of the exocyst in matrix metalloproteinase secretion and actin dynamics during tumor cell invadopodia formation. Mol. Biol. Cell *20*, 3763–3771.

Liu, J., Zhao, Y., Sun, Y., He, B., Yang, C., Svitkina, T., Goldman, Y.E., and Guo, W. (2012). Exo70 stimulates the Arp2/3 complex for lamellipodia formation and directional cell migration. Curr. Biol. *22*, 1510–1515.

Mani, S.A., Guo, W., Liao, M.J., Eaton, E.N., Ayyanan, A., Zhou, A.Y., Brooks, M., Reinhard, F., Zhang, C.C., Shipitsin, M., et al. (2008). The epithelial-mesenchymal transition generates cells with properties of stem cells. Cell *133*, 704–715.

Moskalenko, S., Henry, D.O., Rosse, C., Mirey, G., Camonis, J.H., and White, M.A. (2002). The exocyst is a Ral effector complex. Nat. Cell Biol. *4*, 66–72.

Moskalenko, S., Tong, C., Rosse, C., Mirey, G., Formstecher, E., Daviet, L., Camonis, J., and White, M.A. (2003). Ral GTPases regulate exocyst assembly through dual subunit interactions. J. Biol. Chem. *278*, 51743–51748.

Munson, M., and Novick, P. (2006). The exocyst defrocked, a framework of rods revealed. Nat. Struct. Mol. Biol. *13*, 577–581.

Murphy, D.A., and Courtneidge, S.A. (2011). The 'ins' and 'outs' of podosomes and invadopodia: characteristics, formation and function. Nat. Rev. Mol. Cell Biol. *12*, 413–426.

Nelson, W.J. (2003). Adaptation of core mechanisms to generate cell polarity. Nature *422*, 766–774.

Nieman, M.T., Prudoff, R.S., Johnson, K.R., and Wheelock, M.J. (1999). N-cadherin promotes motility in human breast cancer cells regardless of their E-cadherin expression. J. Cell Biol. *147*, 631–644.

Nieto, M.A. (2011). The ins and outs of the epithelial to mesenchymal transition in health and disease. Annu. Rev. Cell Dev. Biol. *27*, 347–376.

Nürnberg, A., Kitzing, T., and Grosse, R. (2011). Nucleating actin for invasion. Nat. Rev. Cancer *11*, 177–187.

Ohkubo, T., and Ozawa, M. (2004). The transcription factor Snail downregulates the tight junction components independently of E-cadherin downregulation. J. Cell Sci. *117*, 1675–1685.

Oser, M., Yamaguchi, H., Mader, C.C., Bravo-Cordero, J.J., Arias, M., Chen, X., Desmarais, V., van Rheenen, J., Koleske, A.J., and Condeelis, J. (2009). Cortactin regulates cofilin and N-WASp activities to control the stages of invadopodium assembly and maturation. J. Cell Biol. *186*, 571–587.

Pollard, T.D., and Borisy, G.G. (2003). Cellular motility driven by assembly and disassembly of actin filaments. Cell *112*, 453–465.

Polzin, A., Shipitsin, M., Goi, T., Feig, L.A., and Turner, T.J. (2002). Ral-GTPase influences the regulation of the readily releasable pool of synaptic vesicles. Mol. Cell. Biol. *22*, 1714–1722.

Ren, J., and Guo, W. (2012). ERK1/2 regulate exocytosis through direct phosphorylation of the exocyst component Exo70. Dev. Cell *22*, 967–978.

Ridley, A.J. (2011). Life at the leading edge. Cell *145*, 1012–1022.

Rossé, C., Hatzoglou, A., Parrini, M.C., White, M.A., Chavrier, P., and Camonis, J. (2006). RalB mobilizes the exocyst to drive cell migration. Mol. Cell. Biol. *26*, 727–734.

Rosse, C., Formstecher, E., Boeckeler, K., Zhao, Y., Kremerskothen, J., White, M.D., Camonis, J.H., and Parker, P.J. (2009). An aPKC-exocyst complex controls paxillin phosphorylation and migration through localised JNK1 activation. PLoS Biol. *7*, e1000235.

Savagner, P., Vallés, A.M., Jouanneau, J., Yamada, K.M., and Thiery, J.P. (1994). Alternative splicing in fibroblast growth factor receptor 2 is associated with induced epithelial-mesenchymal transition in rat bladder carcinoma cells. Mol. Biol. Cell *5*, 851–862.

Shapiro, I.M., Cheng, A.W., Flytzanis, N.C., Balsamo, M., Condeelis, J.S., Oktay, M.H., Burge, C.B., and Gertler, F.B. (2011). An EMT-driven alternative splicing program occurs in human breast cancer and modulates cellular phenotype. PLoS Genet. *7*, e1002218.

Spiczka, K.S., and Yeaman, C. (2008). Ral-regulated interaction between Sec5 and paxillin targets Exocyst to focal complexes during cell migration. J. Cell Sci. *121*, 2880–2891.

Thapa, N., Sun, Y., Schramp, M., Choi, S., Ling, K., and Anderson, R.A. (2012). Phosphoinositide signaling regulates the exocyst complex and polarized integrin trafficking in directionally migrating cells. Dev. Cell *22*, 116–130.

Thiery, J.P. (2002). Epithelial-mesenchymal transitions in tumour progression. Nat. Rev. Cancer *2*, 442–454.

Thiery, J.P. (2003). Epithelial-mesenchymal transitions in development and pathologies. Curr. Opin. Cell Biol. *15*, 740–746.

Thiery, J.P., Acloque, H., Huang, R.Y., and Nieto, M.A. (2009). Epithelial-mesenchymal transitions in development and disease. Cell *139*, 871–890.

Valastyan, S., and Weinberg, R.A. (2011). Tumor metastasis: molecular insights and evolving paradigms. Cell *147*, 275–292.

Warzecha, C.C., and Carstens, R.P. (2012). Complex changes in alternative pre-mRNA splicing play a central role in the epithelial-to-mesenchymal transition (EMT). Semin. Cancer Biol. *22*, 417–427.

Warzecha, C.C., Sato, T.K., Nabet, B., Hogenesch, J.B., and Carstens, R.P. (2009). ESRP1 and ESRP2 are epithelial cell-type-specific regulators of FGFR2 splicing. Mol. Cell *33*, 591–601.

Warzecha, C.C., Jiang, P., Amirikian, K., Dittmar, K.A., Lu, H., Shen, S., Guo, W., Xing, Y., and Carstens, R.P. (2010). An ESRP-regulated splicing programme is abrogated during the epithelial-mesenchymal transition. EMBO J. *29*, 3286–3300.

Weaver, A.M. (2006). Invadopodia: specialized cell structures for cancer invasion. Clin. Exp. Metastasis *23*, 97–105.

Yamaguchi, H., Lorenz, M., Kempiak, S., Sarmiento, C., Coniglio, S., Symons, M., Segall, J., Eddy, R., Miki, H., Takenawa, T., and Condeelis, J. (2005).

Molecular mechanisms of invadopodium formation: the role of the N-WASP-Arp2/3 complex pathway and cofilin. J. Cell Biol. *168*, 441–452.

Yanagisawa, M., Huveldt, D., Kreinest, P., Lohse, C.M., Cheville, J.C., Parker, A.S., Copland, J.A., and Anastasiadis, P.Z. (2008). A p120 catenin isoform switch affects Rho activity, induces tumor cell invasion, and predicts metastatic disease. J. Biol. Chem. *283*, 18344–18354.

Yang, J., and Weinberg, R.A. (2008). Epithelial-mesenchymal transition: at the crossroads of development and tumor metastasis. Dev. Cell *14*, 818–829.

Yang, J., Mani, S.A., Donaher, J.L., Ramaswamy, S., Itzykson, R.A., Come, C., Savagner, P., Gitelman, I., Richardson, A., and Weinberg, R.A. (2004). Twist, a master regulator of morphogenesis, plays an essential role in tumor metastasis. Cell *117*, 927–939.

Yang, J., Mani, S.A., and Weinberg, R.A. (2006). Exploring a new twist on tumor metastasis. Cancer Res. *66*, 4549–4552.

Yeaman, C., Grindstaff, K.K., and Nelson, W.J. (2004). Mechanism of recruiting Sec6/8 (exocyst) complex to the apical junctional complex during polarization of epithelial cells. J. Cell Sci. *117*, 559–570.

Zárský, V., Cvrcková, F., Potocký, M., and Hála, M. (2009). Exocytosis and cell polarity in plants - exocyst and recycling domains. New Phytol. *183*, 255–272.

Zhao, Y., Liu, J., Yang, C., Capraro, B.R., Baumgart, T., Bradley, R.P., Ramakrishnan, N., Xu, X., Radhakrishnan, R., Svitkina, T., et al. (2013). Exo70 generates membrane curvature for morphogenesis and cell migration. Developmental Cell. *26*, 266–278.

Zuo, X., Zhang, J., Zhang, Y., Hsu, S.C., Zhou, D., and Guo, W. (2006). Exo70 interacts with the Arp2/3 complex and regulates cell migration. Nat. Cell Biol. *8*, 1383–1388.